

LETTERS

Ion permeation through the Na⁺,K⁺-ATPase

Nicolás Reyes¹ & David C. Gadsby¹

P-type ATPase pumps generate concentration gradients of cations across membranes in nearly all cells. They provide a polar transmembrane pathway, to which access is strictly controlled by coupled gates that are constrained to open alternately, thereby enabling thermodynamically uphill ion transport (for example, see ref. 1). Here we examine the ion pathway through the Na⁺,K⁺-ATPase, a representative P-type pump, after uncoupling its extra- and intracellular gates with the marine toxin palytoxin². We use small hydrophilic thiol-specific reagents³ as extracellular probes and we monitor their reactions, and the consequences, with cysteine residues introduced along the anticipated cation pathway through the pump. The distinct effects of differently charged reagents indicate that a wide outer vestibule penetrates deep into the Na⁺,K⁺-ATPase, where the pathway narrows and leads to a charge-selectivity filter. Acidic residues in this region, which are conserved to coordinate pumped ions, allow the approach of cations but exclude anions. Reversing the charge at just one of those positions converts the pathway from cation selective to anion selective. Close structural homology among the catalytic subunits of Ca²⁺-, Na⁺,K⁺- and H⁺,K⁺-ATPases⁴⁻⁶ argues that their extracytosolic cation exchange pathways all share these physical characteristics.

In each transport cycle, up to a hundred times a second, a single Na⁺,K⁺-ATPase pump exchanges three cytoplasmic Na⁺ ions for two extracellular K⁺ ions and hydrolyses one molecule of ATP. Twice per cycle, the gates that allow alternate-side access both close around the bound ions, occluding them deep within the protein. Occlusion of Na⁺ is linked to phosphorylation of the Na⁺,K⁺-ATPase by the ATP molecule hydrolysed, and K⁺ occlusion is linked to dephosphorylation, thereby ensuring vectorial ion transport. Homology models of the Na⁺,K⁺-ATPase α -subunit based on crystal structures of the related Ca²⁺-ATPase^{7,8} suggest sites for the three occluded Na⁺ ions^{5,9} or two occluded K⁺ ions⁵. But the routes taken by ions approaching or leaving these sites remain unclear¹⁰⁻¹².

Palytoxin disrupts the coupling between the two gates of the Na⁺,K⁺ pump, enabling both to sometimes be open at the same time, whereupon the toxin-bound pump becomes a cation channel¹³. Ready reversibility of palytoxin², gating of palytoxin-bound 'pump-channels' by physiological pump ligands², and accessibility of cysteine residues in those channels^{14,15} at positions expected to coordinate transported ions^{5,16} all argue that cations flow through palytoxin-bound pump-channels along a normal transport route. Palytoxin seems to stabilize an E2P-like Na⁺,K⁺ pump conformation (one of the two principal conformations adopted by the pump once it has been phosphorylated) with an open ion pathway¹⁷.

No crystal structure of any E2P-like state with an open ion pathway is available. We therefore generated a homology model of the Na⁺,K⁺-ATPase transmembrane domain (Fig. 1) based on the MgF₄²⁻- and thapsigargin-stabilized Ca²⁺-ATPase structure (E2·MgF₄²⁻ form)¹⁰, even though the structure¹⁰ and functional studies¹² show that its ion pathway is closed. The model has an extracellular cavity, which is bounded on one side by transmembrane

helix 4 (TM4; Fig. 1a, b, blue) and at its bottom by the outer end of TM6 (Fig. 1a, b, green, and Supplementary Fig. 1). To probe the ion pathway, we replaced four strategically located residues (yellow) in TM4 and TM6 one by one with cysteine in ouabain-resistant, *Xenopus laevis* Na⁺,K⁺-ATPase α_1 subunits, which we then expressed in *Xenopus* oocytes.

We briefly exposed outside-out membrane patches to 100 nM palytoxin (Fig. 2a-d, black arrowheads) to transform mutant Na⁺,K⁺ pumps into channels (100 μ M ouabain precluded signals from endogenous *Xenopus* Na⁺,K⁺ pumps), and then tested the accessibility of each engineered cysteine to hydrophilic thiol-specific reagents of similar size³, but bearing either a positive (MTSET⁺, 2-trimethylammonium-ethyl-methanethiosulphonate, blue) or a negative (MTSES⁻, 2-sulphonato-ethyl-methanethiosulphonate, red) charge. The cysteine near the rim of the cavity at the top of TM4 (in mutant E321C) reacted rapidly with both MTSET⁺ and MTSES⁻; cation current through palytoxin-bound pump-channels was decreased about threefold by MTSET⁺ (Fig. 2a, e, left) but was unaltered by MTSES⁻, which nonetheless reacted because it prevented current decrease by MTSET⁺ (Fig. 2a, e, right). MTSET⁺ also reacted rapidly with a cysteine near the end of TM6 (in G805C), again decreasing cation current about threefold (Fig. 2b, e, left), whereas MTSES⁻ almost doubled the current (Fig. 2b, e, right). In contrast, cation current was diminished when the cysteine at the adjacent position (in T806C) was modified by MTSET⁺ (almost completely; Fig. 2c, e, left) or MTSES⁻ (by about a quarter; Fig. 2c, e, right). MTSET⁺ reaction with the deeper cysteine (in G337C) also greatly decreased current (\sim 10-fold; Fig. 2d, e, left), but MTSES⁻ did not react because it neither altered current nor prevented its decrease by MTSET⁺ (Fig. 2d, right).

Rapid reaction with MTSET⁺ suggests that all four cysteines border the ion pathway. Because reaction of MTSES⁻ with cysteines at the two outermost sites (in E321C and G805C) did not decrease current, these residues must line a vestibule wide enough to accommodate the covalent MTSES⁻ adduct (\sim 5 \times 6 \AA ; ref. 3) without sterically preventing cation flow. But the decrease in current caused by MTSES⁻ or MTSET⁺ modification of cysteine at position 806 implies narrowing of the ion pathway at this point. Reaction of MTSET⁺, but not the similarly sized MTSES⁻, with the deeper cysteine at 337 suggests that MTSES⁻ cannot reach that site and, thus, that a cation-selectivity filter may lie between T806 and G337.

Reaction with the neutral, but similarly bulky, reagent MTSACE (2-aminocarbonyl-ethyl-methanethiosulphonate) confirmed the different effects of MTS adducts at G805C and T806C. Current was unchanged by MTSACE reaction with G805C (Fig. 3a, green arrow), which was verified by a subsequent lack of MTSET⁺ effect. But in T806C the neutral MTSACE adduct sharply decreased cation current (\sim 7-fold; Fig. 3b, green arrow), further indicating that the pathway is narrow at position 806.

To rule out changes in pump-channel open probability as explanations for the different effects of MTS reagents in mutants G805C and T806C, we applied MTSES⁻ to single palytoxin-bound

¹Laboratory of Cardiac/Membrane Physiology, The Rockefeller University, New York, New York 10021, USA.

pump-channels (Fig. 3c, d). We used MTSES⁻ because the other reagents both nearly abolished current through T806C pump-channels (Figs 2c, e, and 3b). As in the recordings from hundreds of pump-channels, MTSES⁻ made the single-channel current suddenly increase when the cysteine was at position 805 (Fig. 3c, red arrow), but suddenly decrease when it was at 806 (Fig. 3d, red arrow). Measurements at several potentials confirmed these changes in channel conductance (Fig. 3c–f). We conclude that the wide channel mouth, where MTSES⁻ and MTSACE adducts fit without slowing cation flow, becomes a narrow pore at position 806, where either adduct sterically impedes cation passage.

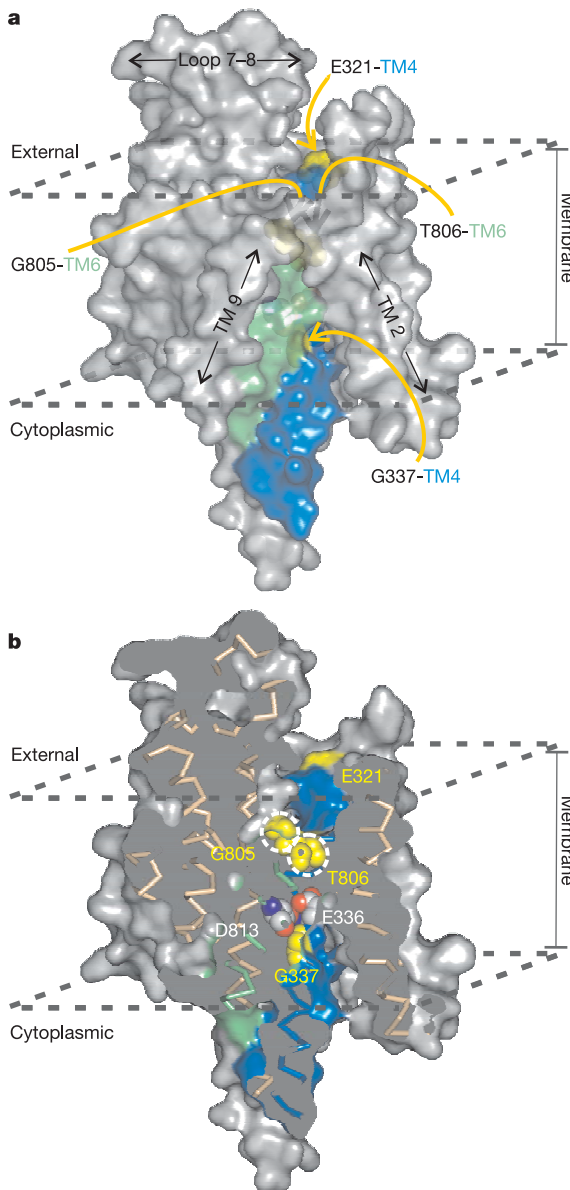


Figure 1 | Homology model of the Na⁺,K⁺-ATPase transmembrane domain. **a**, Model based on the E2·MgF₄⁻ structure of Ca²⁺-ATPase¹⁰ (PDB 1WPG). The outer solvent accessible surface is coloured grey except for TM4 (blue) and TM6 (green). Broken lines indicate approximate membrane surfaces. Four mutated residues (yellow arrows), E321 and G337 in TM4, and G805 and T806 at the top of TM6 (corresponding to Ca²⁺-ATPase residues Y294, G310, I788 and P789), are shown in yellow space-filling notation. G805 and T806 are barely visible through the pseudo-transparent surface. **b**, Vertical cut uncovers an external vestibule, with G805 and T806 near its floor, and reveals residue G337. Residues E336 and D813, equivalent to Ca²⁺-ATPase residues E309 and N796, are also indicated in Corey-Pauling-Kottun-coloured space-filling notation.

Because T806 points at TM4 in the homology model, whereas G805 points away (Supplementary Fig. 2a), orientation relative to TM4 might explain the differences in MTS effects at these positions. In support of this interpretation, the effects of the MTS reagents (MTSET⁺, MTSACE and MTSES⁻) in mutant V807C (Supplementary Fig. 2b), which is also expected to point away from TM4 (Supplementary Fig. 2a), resembled those in G805C. The failure of L802C, P803C, L804C, T808C, I809C, L810C and C811 (native cysteine) palytoxin-bound pump-channels to respond to 1 mM MTSET⁺ (data not shown) hampered further structural analysis.

If a cation-selectivity filter is located between T806 and G337 (Fig. 2), the four acidic residues in that region, E336 in TM4, E788 in TM5, and D813 and D817 in TM6 (Fig. 4a, b, and Supplementary Fig. 3), are obvious candidates to contribute to it. All four, together with the side-chain oxygen of N785, have been implicated, by mutation¹⁶ and modelling^{5,9}, in coordination of transported Na⁺ and K⁺ ions. We replaced each one with cysteine and assessed the

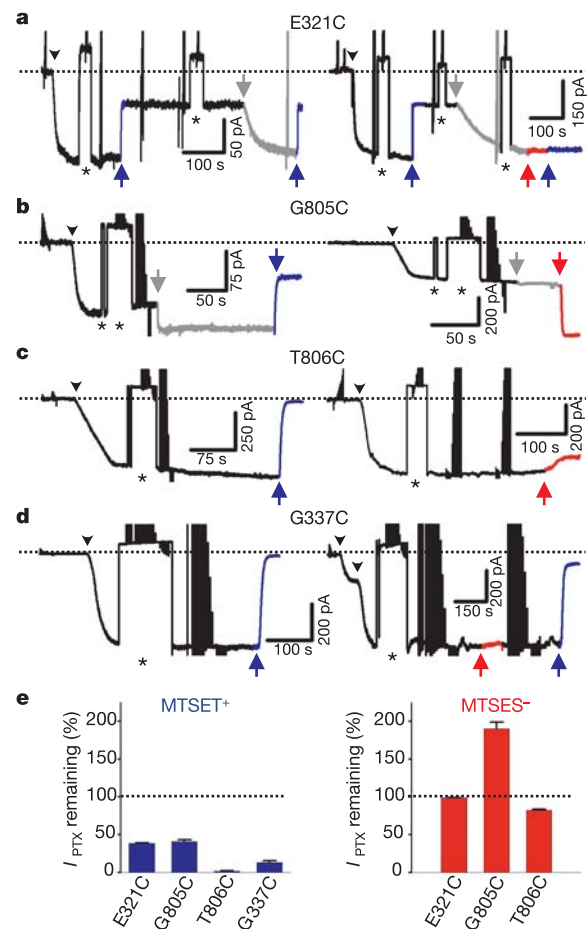


Figure 2 | Effects of MTSET⁺ and MTSES⁻ on E321C, G805C, T806C and G337C mutants. **a–d**, Current at –50 mV in outside-out patches exposed to symmetrical Na⁺ concentrations. Application of 100 nM palytoxin (black arrowheads) for 10–50 s opened hundreds of mutant Na⁺,K⁺ pump-channels, generating a macroscopic inward current (dotted line marks zero palytoxin-induced current, I_{PTX}). Temporary substitution (asterisk) of NMDG⁺ for external Na⁺ monitored patch integrity; 1 mM MTSET⁺ (blue arrows, blue traces) or MTSES⁻ (red arrows, red traces) was applied until the current was steady. Application of 10 mM dithiothreitol (grey arrows, grey traces) either reversed modification by MTSET⁺ by reducing the resulting disulphide bond (**a**), or reverted spontaneous oxidation of engineered cysteines (**b**). **e**, Percentage of I_{PTX} remaining at –50 mV after MTSET⁺ (left, E321C = 38 ± 1%, n = 3; G805C = 41 ± 2%, n = 9; T806C = 2 ± 1%, n = 8; G337C = 13 ± 3%, n = 10) or MTSES⁻ (right, E321C = 99 ± 1%, n = 2; G805C = 190 ± 9%, n = 3; T806C = 82 ± 1%, n = 3) application. All data are the mean ± s.e.m.

cation/anion selectivity of the resulting palytoxin-bound pump-channels by estimating, before and after exposure to 1 mM MTSET⁺, the permeability ratio ($P_{\text{Na}}/P_{\text{NO}_3}$) determined¹⁸ from the reversal potential shift (ΔV_{rev}) of pump-channel current on decreasing external NaNO₃ concentration. Before any cysteine was introduced, ΔV_{rev} was negative (Fig. 4c) and its magnitude matched the change in Na⁺ electrochemical equilibrium potential calculated from the Nernst equation (Fig. 4d, broken line; reproduced in Fig. 4e–g), confirming perfect cation selectivity (that is, $P_{\text{Na}}/P_{\text{NO}_3} \approx \infty$). Three cysteine substitutions, N785C ($n = 5$), E788C ($n = 4$) and D817C ($n = 2$), yielded similarly highly cation-selective pump-channels (Fig. 4e), none of which responded to 1 mM MTSET⁺. For the mutant D813C, however, cation/anion selectivity was decreased ($P_{\text{Na}}/P_{\text{NO}_3} = 8.4 \pm 0.6$, $n = 12$; Fig. 4f, black points and line), and was grossly impaired after MTSET⁺ treatment ($P_{\text{Na}}/P_{\text{NO}_3} = 1.5 \pm 0.2$, $n = 2$; Fig. 4f, blue points and line). Notably,

the TM4 mutant E336C showed greatly decreased cation/anion selectivity ($P_{\text{Na}}/P_{\text{NO}_3} = 2.8 \pm 0.03$, $n = 3$; Fig. 4g, black points and line) and was transformed from cation selective to anion selective by reaction with MTSET⁺ ($P_{\text{Na}}/P_{\text{NO}_3} = 0.2 \pm 0.01$, $n = 3$; Fig. 4g, blue points and lines). We conclude that D813 and E336 both contribute

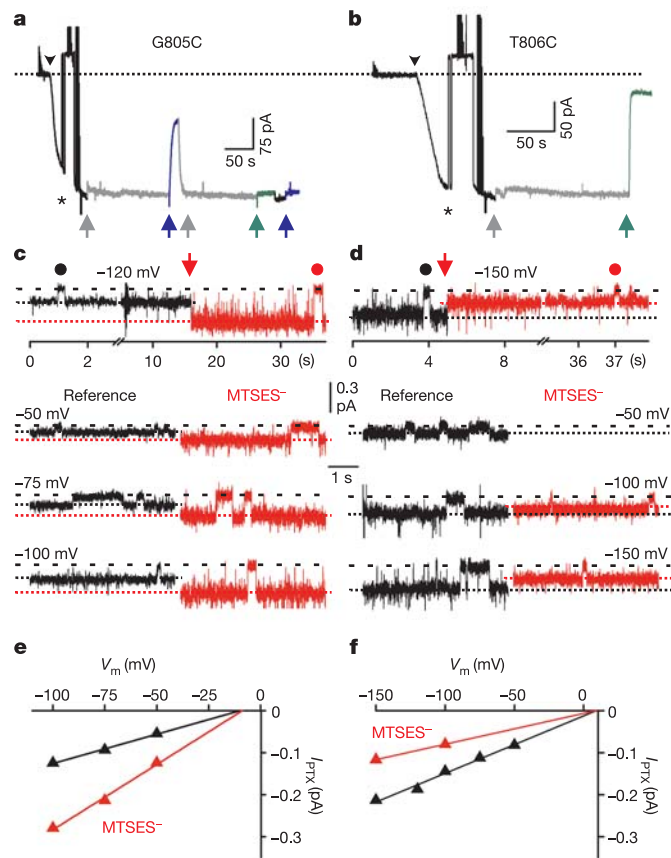


Figure 3 | Analysis of MTS-reagent action on G805C and T806C mutants. **a, b**, Currents measured under the conditions of Fig. 2. Neutral MTSACE at 1 mM (green arrows, green traces) did not alter current in G805C ($n = 3$), but greatly decreased it in T806C (% I_{PTX} remaining after MTSACE, $14 \pm 2\%$; $n = 3$) pumps. **c, d**, Outside-out patches were exposed to 100 pM palytoxin until a single G805C (**c**) or T806C (**d**) pump-channel opened. After recording channel closures (black dots), MTSES⁻ action (red arrows) on single open channels increased (G805C) or decreased (T806C) both the open-channel current (dotted lines) and the amplitudes of subsequent closure events (red dots). **e, f**, Linear fits to microscopic I_{PTX} amplitude measurements at the voltages indicated (**c, d**) yielded conductance values for G805C (**e**) of 1.4 pS before (black) and 3.1 pS after (red) MTSES⁻ application, and for T806C (**f**) of 1.4 pS before (black) and 0.7 pS after (red) MTSES⁻ application. For T806C, the % macroscopic I_{PTX} remaining after MTSES⁻ application in the experiments of Fig. 2e, right, was 57 ± 2% ($n = 3$) when measured at -150 mV; this good correlation between macroscopic and microscopic data is expected given the high open probability (~0.9) of G805C (**c**) and T806C (**d**) pump-channels. All data are the mean ± s.e.m.

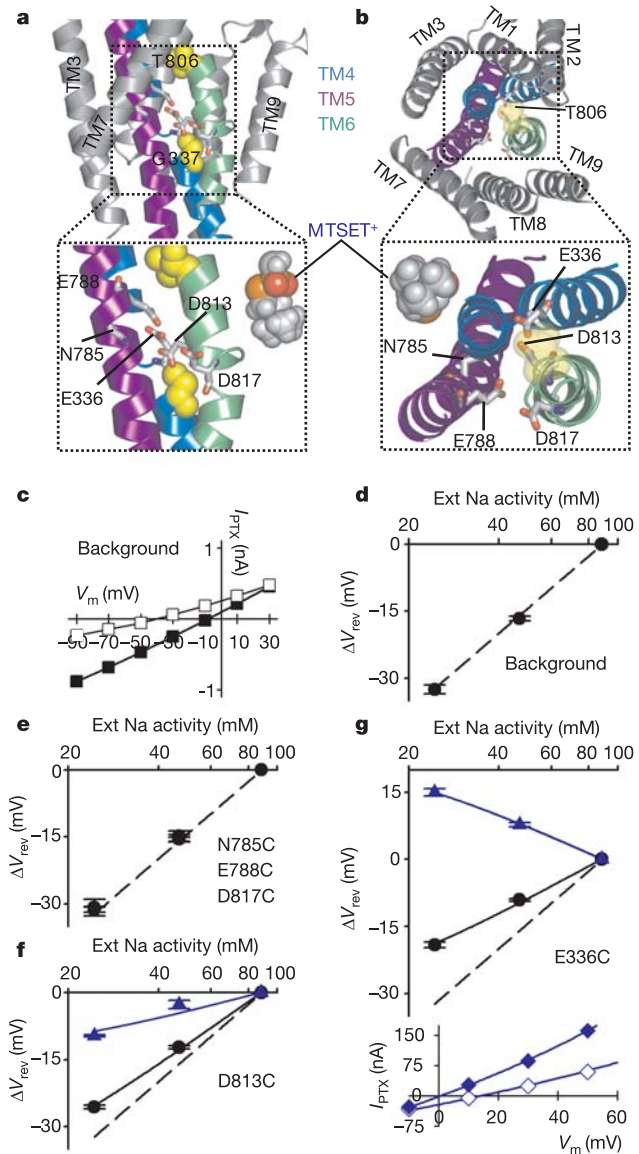


Figure 4 | Charge selectivity in palytoxin-bound pump-channels. **a, b**, Na⁺, K⁺ pump homology model (Fig. 1) viewed parallel to the membrane plane (**a**) or from the extracellular surface (**b**), with MTSET⁺ shown for size reference. **c**, Pump-channels retaining all indicated native residues (Background) showed a large negative shift of V_{rev} on decreasing external NaNO₃ concentration (filled squares, 120 mM; open squares, 30 mM). **d–g**, Semi-log plots of ΔV_{rev} versus external Na⁺ activity. Results from background pump-channels (**d**) and from N785C, E788C or D817C mutants (**e**) approximate the broken line, which is appropriate to exclusive cation selectivity and calculated as $\Delta E_{\text{rev}} = (RT/F)\ln(X)$, where X is the ratio of the lower to the higher monovalent cation activity. Mutations D813C (**f**) and E336C (**g**) each weakened cation-to-anion selectivity (black circles and fit lines). MTSET⁺ treatment (blue triangles and fit lines) further impaired the cation selectivity of D813C channels (**f**) and rendered E336C channels (**g**) anion selective; inset in **g** shows the positive ΔV_{rev} due to a fourfold decrease in external NaNO₃ concentration (filled to open blue diamonds) in MTSET⁺-modified E336C channels. Residues corresponding to E336, N785, E788, D813 and D817 in the Ca²⁺-ATPase are E309, N768, E771, N796 and D800. Error bars indicate the s.e.m.

to the strong cation selectivity of palytoxin-bound pump–channels, which is impaired when either negative charge is attenuated (by mutation to cysteine) and is further compromised (position 813) or switched to anion selectivity (position 336) when a positive charge is added (by reaction with MTSET⁺).

Our results show that extracellular ions enter Na⁺,K⁺ pump–channels through a wide vestibule that extends to the hydrophobic core of the membrane before suddenly narrowing to form a cation-selective pore. The principal cation-selectivity determinants are acidic residues expected to form binding sites in which Na⁺ and K⁺ ions are normally occluded. Evidence suggests that this architecture is conserved in the related H⁺,K⁺- and Ca²⁺-ATPases, and in Na⁺,K⁺-ATPase without palytoxin. An external cavity observed in electron microscopic images of thapsigargin-stabilized E2-like Ca²⁺-ATPase¹⁹ has been confirmed in crystal structures of E2P-related Ca²⁺-ATPase forms (E2·AlF₄⁻, ref. 20; E2·MgF₄²⁻, ref. 10). E2P forms of Na⁺,K⁺ and H⁺,K⁺ pumps also apparently include an external cavity large enough to accommodate bulky extracellular inhibitors such as the cardiotonic steroid ouabain (Na⁺,K⁺ pump) or omeprazole (H⁺,K⁺ pump): both bind to E2P conformations^{6,21,22}; and high-affinity binding of ouabain requires T806 of Na⁺,K⁺-ATPase (for example, see ref. 21), whereas omeprazole covalently binds to the T806-equivalent residue C813 of the H⁺,K⁺ pump (for example, see refs 6, 22).

The fact that a narrow access channel connects ion-binding sites in the Na⁺,K⁺ pump to the extracellular solution has been inferred from the membrane-potential dependence of extracellular Na⁺ and K⁺ action (for example, see ref. 23). In addition, a narrow fissure in the E2·MgF₄²⁻ structure, penetrating from the T806-equivalent residue (P789) of the Ca²⁺-ATPase towards Ca²⁺-binding site II, has been proposed as a possible exit route for released Ca²⁺ (ref. 10; but see also refs 11, 12). At binding site II, between TM4 and TM6 in the E1·2Ca²⁺ structure⁷, side-chain oxygen atoms of residues equivalent to E336 (E309) and D813 (N796) coordinate Ca²⁺. E336 and D813 are therefore modelled as components of the corresponding Na⁺,K⁺ pump site, alternately coordinating Na⁺ ions in E1 and a K⁺ ion in E2 conformations^{5,9}, and their key roles in both Na⁺,K⁺- and Ca²⁺-ATPases are corroborated by the functional consequences of mutating them^{16,24,25}. We found that palytoxin-bound pump–channels with cysteine substitutions at N785, E788 or D817—also modelled to coordinate occluded Na⁺ and K⁺ ions⁵—remained highly cation selective and unresponsive to extracellular 1 mM MTSET⁺. This might reflect rearrangement of the coordinating sites when the ion pathway opens. Binding-site structure indeed differs between the Ca²⁺-bound⁷ and unbound deoccluded^{10,11} Ca²⁺-ATPase states. In the latter only side chains of the E336- and D813-equivalent residues occupy the space between TM4 and TM6 (compare Fig. 4b and Supplementary Figs 3 and 4), whereas in the former the D817-equivalent side chain also enters this space (Supplementary Fig. 4). Our results imply that in an open E2P-like state, with ion-binding sites accessible from the extracytoplasmic side of the membrane, the arrangement of coordinating residues resembles that in the deoccluded E2P-related structures^{10,11,20}.

We conclude that, in the E2P conformation of the Na⁺,K⁺ pump, Na⁺ and K⁺ exchange between site II and the external medium occurs through a funnel-shaped pathway, which is lined in part by TM4 and TM6 and comprises a cation-selectivity filter formed by acidic residues in the ion-coordination site. We propose that the extracytoplasmic ion exchange pathways of Ca²⁺-, H⁺,K⁺- and Na⁺,K⁺-ATPase cation pumps share these physical characteristics. These methods should facilitate further characterization of the ion translocation pathway of the Na⁺,K⁺ pump, including the locations of the gates that control access to the ion-binding sites.

METHODS

Model building. The *Xenopus* Na⁺,K⁺-ATPase α_1 subunit homology model was built from the Ca²⁺-ATPase E2·MgF₄²⁻ structure¹⁰ (PDB code 1WPG) with

SWISS-MODEL (<http://swissmodel.expasy.org>). Structural figures were prepared with PyMOL version 0.97 (<http://www.pymol.org>).

Ouabain- and MTS-insensitive Na⁺,K⁺ pumps. Na⁺,K⁺ pumps insensitive to ouabain²⁶ and MTS reagents¹⁴ were made by introducing the point mutations Q120D, N131R and C113S into *Xenopus* α_1 subunits²⁷. All other mutations were introduced into these Q120D-N131R-C113S Na⁺,K⁺ pumps, which generate robust extracellular-K⁺-activated currents in Na⁺-loaded oocytes (data not shown). Complementary RNAs of mutant *Xenopus* α_1 catalytic and wild-type *Xenopus* β_3 auxiliary subunits²⁸ were coinjected in a 2:1 ratio into *Xenopus* oocytes. The mutation N131R decreased the conductance of single palytoxin-bound pump–channels to ~1.5 pS, as compared with ~4 pS for the wild-type (N131) channel²⁹.

Current recordings. Macroscopic or microscopic currents were recorded at 22–24°C in outside-out patches excised from *Xenopus* oocytes, 1–3 d after injection. Internal (pipette) solutions contained (in mM): 120 NaOH, 90 sulphamic acid, 1 MgCl₂, 10 HEPES and 10 EGTA. External solutions contained (in mM): 120 NaOH or *N*-methyl-D-glucamine (NMDG), 133 sulphamic acid, 5 Ba(OH)₂, 0.5 Ca(OH)₂, 1 Mg(OH)₂ and 10 HEPES. Palytoxin was added to external 120 mM Na⁺ solutions at concentrations of 100 nM for macroscopic, or 100 pM for microscopic, recording. All external solutions contained 100 μ M ouabain to preclude palytoxin-induced responses from endogenous pumps.

Cation/anion selectivity. For experiments varying Na⁺ activity, sulphamic acid was replaced by nitric acid and sucrose was added to maintain osmolality (250 \pm 10 mosmol kg⁻¹). P_{Na}/P_{NO_3} ratios were obtained by fitting the Goldman–Hodgkin–Katz equation, $V_{rev} = RT/F \cdot \ln\{(P_{Na}/P_{NO_3})[Na^+]_o + [NO_3^-]_i\} / (P_{Na}/P_{NO_3}[Na^+]_i + [NO_3^-]_o)$, where the subscripts o and i indicate external and internal ion activities³⁰, respectively, to values of ΔV_{rev} as a function of Na⁺ and NO₃⁻ activity. All data are reported as the mean \pm s.e.m.

Received 31 May; accepted 26 July 2006.

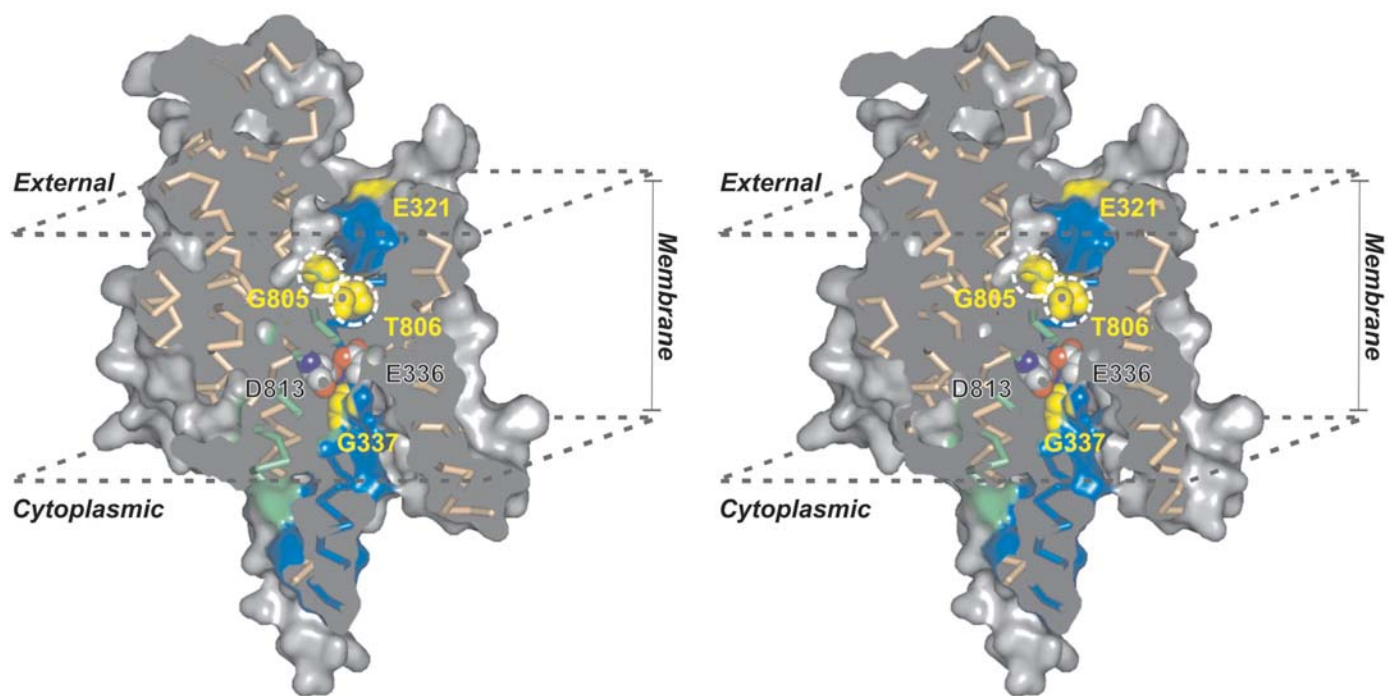
1. Lauger, P. *Electrogenic Ion Pumps* (Sinauer, Sunderland, Massachusetts, 1991).
2. Artigas, P. & Gadsby, D. C. Na⁺/K⁺-pump ligands modulate gating of palytoxin-induced ion channels. *Proc. Natl Acad. Sci. USA* **21**, 501–505 (2003).
3. Karlin, A. & Akabas, M. H. Substituted-cysteine accessibility method. *Methods Enzymol.* **293**, 123–145 (1998).
4. Sweadner, K. J. & Donnet, C. Structural similarities of Na,K-ATPase and SERCA, the Ca²⁺-ATPase of the sarcoplasmic reticulum. *Biochem. J.* **356**, 685–704 (2001).
5. Ogawa, H. & Toyoshima, C. Homology modeling of the cation binding sites of Na⁺/K⁺-ATPase. *Proc. Natl Acad. Sci. USA* **99**, 15977–15982 (2002).
6. Munson, K., Garcia, R. & Sachs, G. Inhibitor and ion binding sites on the gastric H,K-ATPase. *Biochemistry* **44**, 5267–5284 (2005).
7. Toyoshima, C., Nakasako, M., Nomura, H. & Ogawa, H. Crystal structure of the calcium pump of sarcoplasmic reticulum at 2.6 Å resolution. *Nature* **405**, 647–655 (2000).
8. Toyoshima, C. & Nomura, H. Structural changes in the calcium pump accompanying the dissociation of calcium. *Nature* **418**, 605–611 (2002).
9. Rakowski, R. F. & Sagar, S. Found: Na⁺ and K⁺ binding sites of the sodium pump. *News Physiol. Sci.* **18**, 164–168 (2003).
10. Toyoshima, C., Nomura, H. & Tsuda, T. Luminal gating mechanism revealed in calcium pump crystal structures with phosphate analogues. *Nature* **432**, 361–368 (2004).
11. Moller, J. V., Nissen, P., Sorensen, T. L.-M. & le Marie, M. Transport mechanism of the sarcoplasmic reticulum Ca²⁺-ATPase pump. *Curr. Opin. Struct. Biol.* **15**, 387–393 (2005).
12. Picard, M., Toyoshima, C. & Champel, P. Effects of inhibitors on luminal opening of Ca²⁺ binding sites in an E2P-like complex of sarcoplasmic reticulum Ca²⁺-ATPase with Be²⁺-fluoride. *J. Biol. Chem.* **281**, 3360–3369 (2006).
13. Scheiner-Bobis, G., Meyer zu Heringdorf, D., Christ, M. & Habermann, E. Palytoxin induces K⁺ efflux from yeast cells expressing the mammalian sodium pump. *Mol. Pharmacol.* **45**, 1132–1136 (1994).
14. Guennoun, S. & Horisberger, J.-D. Structure of the 5th transmembrane segment of the Na,K-ATPase α subunit: a cysteine-scanning mutagenesis study. *FEBS Lett.* **482**, 144–148 (2000).
15. Horisberger, J.-D. Recent insights into the structure and mechanism of the sodium pump. *Physiology (Bethesda)* **19**, 377–387 (2004).
16. Nielsen, J. M., Pedersen, P. A., Karlsh, S. J. & Jorgensen, P. L. Importance of intramembrane carboxylic acids for occlusion of K⁺ ions at equilibrium in renal Na,K-ATPase. *Biochemistry* **37**, 1961–1968 (1998).
17. Artigas, P. & Gadsby, D. C. Large diameter of palytoxin-induced Na/K pump channels and modulation of palytoxin interaction by Na/K pump ligands. *J. Gen. Physiol.* **123**, 357–376 (2004).
18. Keramidas, A., Moorhouse, A. J., Schofield, P. R. & Barry, P. H. Ligand-gated ion channels: mechanisms underlying ion selectivity. *Prog. Biophys. Mol. Biol.* **86**, 161–204 (2004).
19. Zhang, P., Toyoshima, C., Yonekura, K., Green, N. M. & Stokes, D. L. Structure of the calcium pump from sarcoplasmic reticulum at 8-Å resolution. *Nature* **392**, 835–839 (1998).

20. Olesen, C., Sorensen, T. L., Nielsen, R. C., Moller, J. V. & Nissen, P. Dephosphorylation of the calcium pump coupled to counterion occlusion. *Science* **306**, 2251–2255 (2004).
21. Qiu, L. Y., Koenderink, J. B., Swarts, H. G., Willems, P. H. & De Pont, J. J. Phe⁷⁸³, Thr⁷⁹⁷, and Asp⁸⁰⁴ in transmembrane hairpin M5–M6 of Na⁺,K⁺-ATPase play a key role in ouabain binding. *J. Biol. Chem.* **278**, 47240–47244 (2003).
22. Asano, S. *et al.* The cavity structure for docking the K⁺-competitive inhibitors in the gastric proton pump. *J. Biol. Chem.* **279**, 13968–13975 (2004).
23. Apell, H. J. Structure–function relationship in P-type ATPases—a biophysical approach. *Rev. Physiol. Biochem. Pharmacol.* **150**, 1–35 (2003).
24. Vilsen, B. & Andersen, J. P. Mutation to the glutamate in the fourth membrane segment of Na⁺,K⁺-ATPase and Ca²⁺-ATPase affects cation binding from both sides of the membrane and destabilizes the occluded enzyme forms. *Biochemistry* **37**, 10961–10971 (1998).
25. Inesi, G., Ma, H., Lewis, D. & Xu, C. Ca²⁺ occlusion and gating function of Glu³⁰⁹ in the ADP-fluoroaluminate analog of the Ca²⁺-ATPase phosphoenzyme intermediate. *J. Biol. Chem.* **279**, 31629–31637 (2004).
26. Price, E. M., Rice, D. A. & Lingrel, J. B. Structure–function studies of Na,K-ATPase: site-directed mutagenesis of the border residues from the H1–H2 extracellular domain of the α subunit. *J. Biol. Chem.* **265**, 6638–6641 (1990).
27. Verrey, F. *et al.* Primary sequence of *Xenopus laevis* Na⁺-K⁺-ATPase and its localization in A6 kidney cells. *Am. J. Physiol.* **256**, F1034–F1043 (1989).
28. Good, P. J., Richter, K. & Dawid, I. B. A nervous system-specific isotype of the β subunit of Na⁺,K⁺-ATPase expressed during early development of *Xenopus laevis*. *Proc. Natl Acad. Sci. USA* **87**, 9088–9092 (1990).
29. Artigas, P. & Gadsby, D. C. Ouabain affinity determining residues lie close to the Na/K pump ion pathway. *Proc. Natl Acad. Sci. USA* **103**, 12613–12618 (2006).
30. Grenthe, I., Plyasunov, A. V. & Spahiu, K. In *Modelling in Aquatic Chemistry* (eds Grenthe, I. & Puigdomenech, I.) 325–426 (Organisation for Economic Co-operation and Development (OECD) Publications, Paris, 1997).

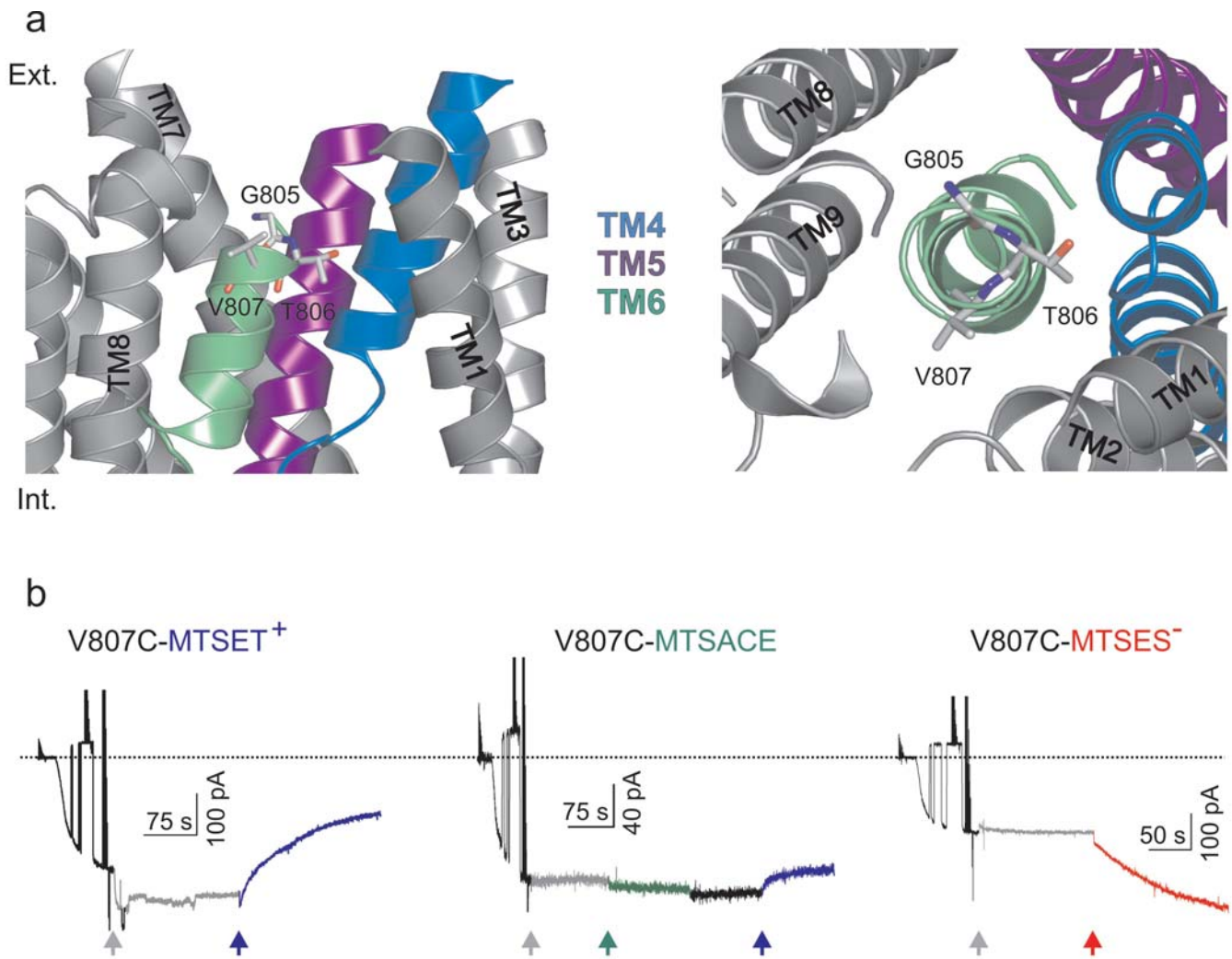
Supplementary Information is linked to the online version of the paper at www.nature.com/nature.

Acknowledgements We thank P. Artigas for advice and discussion; M. Mense and P. Vergani for discussion; and R.F. Rakowski for cDNAs encoding the *Xenopus* α_1 and β Na⁺,K⁺-ATPase subunits. This work was supported by a grant from the NIH (to D.C.G.).

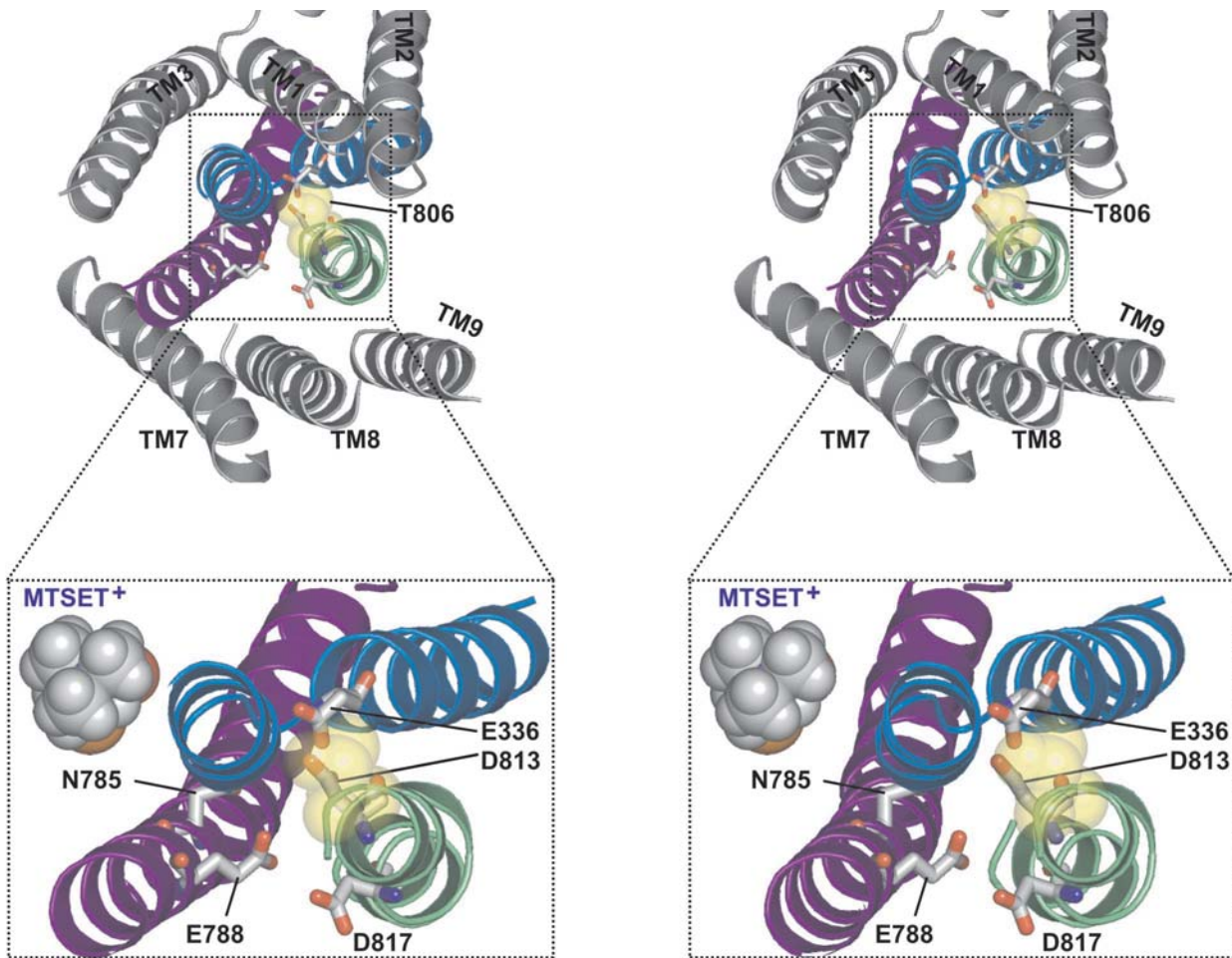
Author Information Reprints and permissions information is available at www.nature.com/reprints. The authors declare no competing financial interests. Correspondence and requests for materials should be addressed to D.C.G. (gadsby@rockefeller.edu).



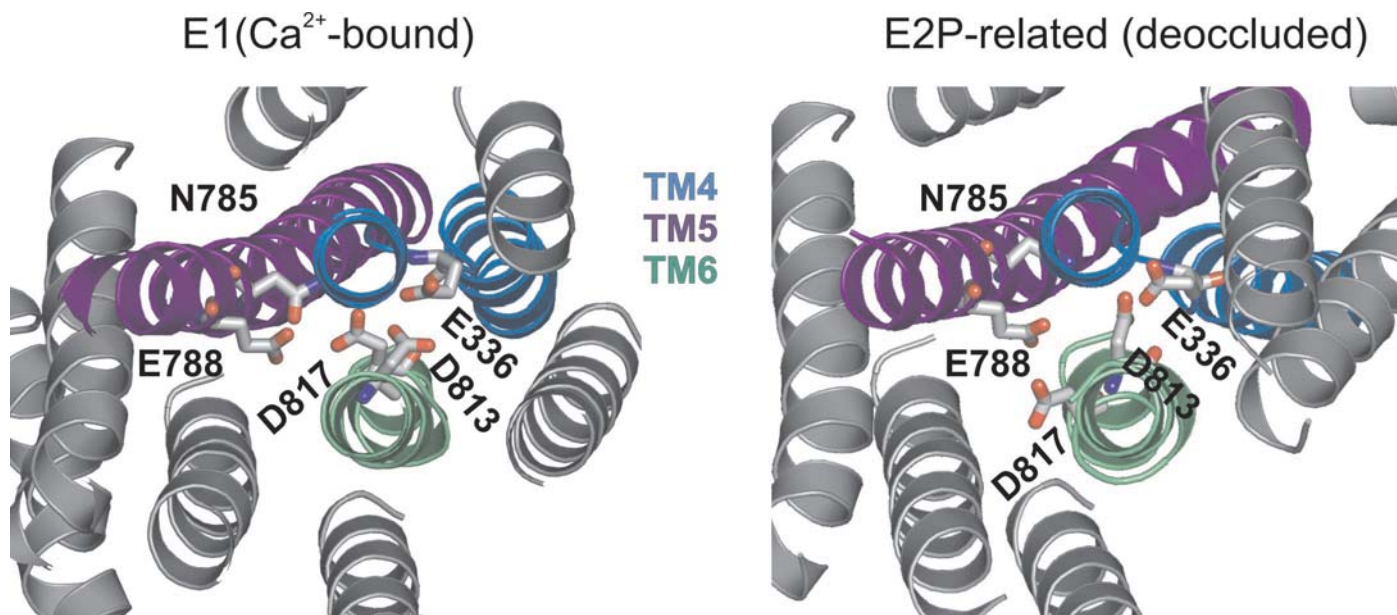
Supplementary Figure S1 Stereo view of the Na⁺,K⁺-ATPase transmembrane-domain homology model depicted in Fig.1b.



Supplementary Figure S2 Effects of differently-charged MTS reagents on V807C mutant. **a**, Views of the Na⁺,K⁺-ATPase homology model (e.g. Fig. 1) parallel to the membrane plane (**left**), and from the extracellular surface (**right**). **b**, Macroscopic currents measured under the conditions of Fig. 2 in outside-out patches containing V807C pump-channels. The percent palytoxin-induced current remaining after MTSET⁺, MTSACE and MTSES⁻ averaged 38±5% (n=3), 106±5% (n=3) and 172±8% (n=5), respectively. Reaction of the neutral MTSACE, was confirmed by subsequent application of a positively charged reagent.



Supplementary Figure S3 Stereo view of the Na⁺,K⁺-ATPase transmembrane-domain homology model depicted in Fig.4b. Note the alignment of residues T806, D813 and E336 along the proposed ion pathway.



Supplementary Figure S4 E1 and E2P-related Na⁺,K⁺-ATPase homology models. Extracellular views show homology models based on Ca²⁺-bound (Toyoshima et al. 2000) (left) and unbound, deoccluded (Toyoshima et al. 2004) (right) crystal structures of the Ca²⁺-ATPase.

Supplementary Methods

Before building the homology model of the *Xenopus* Na⁺,K⁺-ATPase α_1 subunit on the basis of the Ca²⁺-ATPase E2•MgF₄²⁻ structure (PDB accession code 1WPG)¹⁰, the Na⁺,K⁺- and Ca²⁺-ATPase primary sequences were aligned as described⁵ and then adjusted manually. The model was built using the SWISS-MODEL server (<http://swissmodel.expasy.org>), including energy minimization with GROMOS96, and evaluated with Swiss-PdbViewer v 3.7.

We used the *Xenopus* α_1 subunit²⁷ containing the double mutation Q120D-N131R, shown to increase the dissociation constant of ouabain, from ~150 nM to ~5 mM, in sheep Na⁺,K⁺-ATPase²⁶; in control experiments, 10 μ M ouabain sufficed to prevent detection of any palytoxin-induced current from native *Xenopus* $\alpha_1\beta_3$ Na⁺,K⁺ pumps in non-injected oocytes. Addition of a third mutation, C113S (ref. 14), rendered the resulting palytoxin-bound pump-channels (Q120D-N131R-C113S) insensitive to even mM concentrations of MTSET⁺ or MTSES⁻. All other mutations were introduced into this Q120D-N131R-C113S background, which generates robust extracellular-K⁺-activated Na⁺,K⁺ pump currents in Na⁺-loaded oocytes.

Currents were recorded using an Axopatch 200B amplifier, Digidata 1200 A/D board and pCLAMP 7 software (Axon Instruments, Inc.), and were filtered at 0.1–1 kHz (Frequency Devices) and sampled at 1–10 kHz. Currents were also continuously recorded on VCR tape. Single-channel current amplitudes (Fig. 3e,f) were obtained as the separations of peaks of gaussians fitted to all-points histograms constructed (Clampfit 9, pClamp 9) from single-channel recordings.

For all internal and external solutions pH=7.40±0.01 and osmolality=250±10 mosmol/kg. Membrane potentials were corrected for liquid junction potentials (≤ 2.2 mV; calculated with Clampex7). Na⁺ and NO₃⁻ activities (Fig. 4d-g) were determined from NaNO₃ concentrations and mean activity coefficients calculated using the Brønsted-Guggenheim-Scatchard approach³⁰ (the resulting activity coefficients were 0.735, 0.781 and 0.813 for 120, 60 and 30 mM NaNO₃ concentrations, respectively). Ultra-fast solution exchange ($\tau \sim 1$ ms) was achieved by delivering solutions through the two barrels of a theta tube mounted on a piezoelectric-driven switcher (LSS 3200, Burleigh Instruments, Inc).